Angiogenesis (2023) 26:493–503
https://doi.org/10.1007/s10456-023-09881-w

BRIEF COMMUNICATION

Localized conditional induction of brain arteriovenous malformations in a mouse model of hereditary hemorrhagic telangiectasia

Lea Scherschinski[1,2,3] · Chul Han[1] · Yong Hwan Kim[1] · Ethan A. Winkler[1,2] · Joshua S. Catapano[2] · Tyler D. Schriber[1] · Peter Vajkoczy[3] · Michael T. Lawton[1,2] · S. Paul Oh[1]

Received: 21 March 2023 / Accepted: 30 April 2023 / Published online: 23 May 2023

Abstract

Background Longitudinal mouse models of brain arteriovenous malformations (AVMs) are crucial for developing novel therapeutics and pathobiological mechanism discovery underlying brain AVM progression and rupture. The sustainability of existing mouse models is limited by ubiquitous Cre activation, which is associated with lethal hemorrhages resulting from AVM formation in visceral organs. To overcome this condition, we developed a novel experimental mouse model of hereditary hemorrhagic telangiectasia (HHT) with CreER-mediated specific, localized induction of brain AVMs.

Methods Hydroxytamoxifen (4-OHT) was stereotactically delivered into the striatum, parietal cortex, or cerebellum of $R26^{CreER}$; $Alk1^{2f/2f}$ (*Alk1*-iKO) littermates. Mice were evaluated for vascular malformations with latex dye perfusion and 3D time-of-flight magnetic resonance angiography (MRA). Immunofluorescence and Prussian blue staining were performed for vascular lesion characterization.

Results Our model produced two types of brain vascular malformations, including nidal AVMs (88%, 38/43) and arteriovenous fistulas (12%, 5/43), with an overall frequency of 73% (43/59). By performing stereotaxic injection of 4-OHT targeting different brain regions, *Alk1*-iKO mice developed vascular malformations in the striatum (73%, 22/30), in the parietal cortex (76%, 13/17), and in the cerebellum (67%, 8/12). Identical application of the stereotaxic injection protocol in reporter mice confirmed localized Cre activity near the injection site. The 4-week mortality was 3% (2/61). Seven mice were studied longitudinally for a mean (SD; range) duration of 7.2 (3; 2.3−9.5) months and demonstrated nidal stability on sequential MRA. The brain AVMs displayed microhemorrhages and diffuse immune cell invasion.

Conclusions We present the first HHT mouse model of brain AVMs that produces localized AVMs in the brain. The mouse lesions closely resemble the human lesions for complex nidal angioarchitecture, arteriovenous shunts, microhemorrhages, and inflammation. The model's longitudinal robustness is a powerful discovery resource to advance our pathomechanistic understanding of brain AVMs and identify novel therapeutic targets.

Keywords Activin receptor-like kinase 1 · Brain arteriovenous malformation · Hemorrhage · Hereditary hemorrhagic telangiectasia · Magnetic resonance imaging · Mouse model · Stereotaxic

Abbreviations

AVF	Arteriovenous fistula
AVM	Arteriovenous malformation
Alk1	Activin receptor-like kinase 1
Eng	Endoglin
HHT	Hereditary hemorrhagic telangiectasia
iKO	inducible knockout
MRA	Magnetic resonance angiography
MRI	Magnetic resonance imaging
4-OHT	4-Hydroxytamoxifen
PB	Phosphate buffer
PBS	Phosphate-buffered saline

Portions of this manuscript were presented orally at the 14th HHT International Scientific Conference, September 28, 2022, to October 2, 2022, Estoril, Cascais, Portugal; the annual meeting of the Congress of Neurological Surgeons, October 8–12, 2022, San Francisco, California; the 22nd International Vascular Biology Meeting, October 13–17, 2022, Oakland, California; the 91st annual meeting of the American Association of Neurological Surgeons, April 21–24, 2023, Los Angeles, California.

S. Paul Oh and Michael T. Lawton served as co-senior authors and contributed equally to the work.

Extended author information available on the last page of the article

Smad4 *Caenorhabditis elegans Sma* genes fused with *Drosophila* Mad4 [Mothers against decapentaplegic homolog 4]
VEGF Vascular endothelial growth factor

Introduction

Brain arteriovenous malformations (AVMs) represent a leading cause of hemorrhagic stroke in young adults [1, 2]. The AVM angioarchitecture is complex and comprises a high-pressure, low-resistance nidus of dysplastic blood vessels prone to spontaneous rupture and intracranial hemorrhage [3, 4]. Hereditary hemorrhagic telangiectasia (HHT, Osler–Weber–Rendu syndrome) is an autosomal-dominant vascular disorder caused by heterozygous loss-of-function mutations in activin receptor-like kinase 1 (*ALK1*), endoglin (*ENG*), or *SMAD4* [5, 6]. Pathognomic characteristics of HHT include the development of mucocutaneous telangiectasias and AVMs in the lungs, liver, and brain, with up to 20% of HHT patients exhibiting cerebral vascular malformations [6, 7].

Mouse models have provided valuable insights into the underlying genetic mechanisms of HHT and have served as the foundation for genetic-based approaches to generate animal models that simulate human conditions [8]. In the past, animal models of HHT have been engineered for homozygous or heterozygous *Alk1* or *Eng* gene knockout. This approach is limited by high rates of in utero mortality or low rates of AVM formation that disrupt AVM reproduction and preclude longitudinal studies [9, 10]. Recent advances in HHT studies have targeted Cre-mediated time-dependent or tissue-specific deletions (or both) of *Eng*, *Alk1*, or *Smad4*, either through systemic Cre activation or focal delivery of Cre-expressing adenoviral vectors [11–15]. Although these models have been instrumental in advancing our mechanistic understanding of disease pathology, several factors limit the value of current mouse models of HHT. These factors include a lack of specificity, with development of randomly located AVMs in the body [12], high rates of early lethality due to gastrointestinal hemorrhage [12], or the lack of a true vascular nidus [14, 16].

To address these limitations, we developed a novel experimental mouse model of HHT using targeted local drug delivery to induce brain AVMs in specific brain regions of *Alk1*-inducible knockout (*Alk1*-iKO) mice. Our model produced brain AVMs with high consistency and close resemblance to the phenotypical hallmarks of human pathology while obviating the off-target effects commonly associated with systemic HHT gene deletion. Furthermore, the model's ability to recapitulate disease progression over time makes it an invaluable tool for understanding the pathogenesis of brain AVMs and accelerating the development of new and effective therapeutics for individuals affected by HHT.

Methods

Detailed experimental procedures are available in the supplemental methods.

Results

Localized induction of brain AVMs

To develop a novel mouse model of brain AVMs with targeted intracerebral lesion induction, we performed stereotaxic intracerebral injection of 4-hydroxytamoxifen (4-OHT) on postnatal day 1 (P1) in *Alk1*-iKO mice and their control littermates. We evaluated them for vascular lesions 3–4 weeks postinjection using latex dye perfusion. We targeted multiple mouse brain regions with distinct spatial distributions to investigate the spatial relationship of vascular lesion formation relative to the injection site. We targeted the right-hemispheric striatum, the left-hemispheric parietal cortex, and the midline cerebellum (Supplemental Table 1). Stereotaxic injection of 4-OHT into the brain target regions in *Alk1*-iKO mice produced brain vascular lesions in the striatum in 73% (nidal AVM, 82% [18/22]; arteriovenous fistula [AVF], 18% [4/22]) of brains, in the parietal cortex in 76% (nidal AVM, 92% [12/13]; AVF 8% [1/13]), and in the cerebellum in 67% (nidal AVM, 100% [8/8]) (Fig. 1a–d). Among all *Alk1*-iKO mice injected intracerebrally with 4-OHT ($n=59$, female sex, 33 [56%]), 73% (43/59) developed brain vascular malformations, including nidal brain AVMs (88%, 38/43) and AVFs (12%, 5/43). 4-OHT—injected CreER-negative littermates served as negative controls and did not form brain vascular lesions ($n=40$) (Supplemental Fig. 1). The 4-week mortality was 3% (2/61). Both mice developed extensive intracranial hemorrhages from spontaneous brain AVM rupture.

To characterize the vascular lesions produced by our technique, we measured the nidus size and lesion depth in coronal brain tissue sections (Fig. 1e and f). The cumulative mean (SD; range) nidus size of all brain AVMs was 2.33 (1.16; 0.5–4.8) mm, and the mean (SD; range) lesion depth was 1.85 (0.86; 0.45–3.5) mm. Brain AVMs were largest in the striatum with a mean (SD) nidus size of 2.53 (1.0) mm, followed by parietocortical AVMs at 2.28 (1.35) mm and cerebellar AVMs with 1.85 (1.27) mm (Fig. 1e). The mean (SD) lesion depth varied significantly between striatal and parietocortical brain AVMs (2.36 [0.79] mm vs. 1.03 [0.44] mm, $p<0.001$) and between cerebellar and parietocortical AVMs (1.93 [0.35] mm vs. 1.03 [0.44]

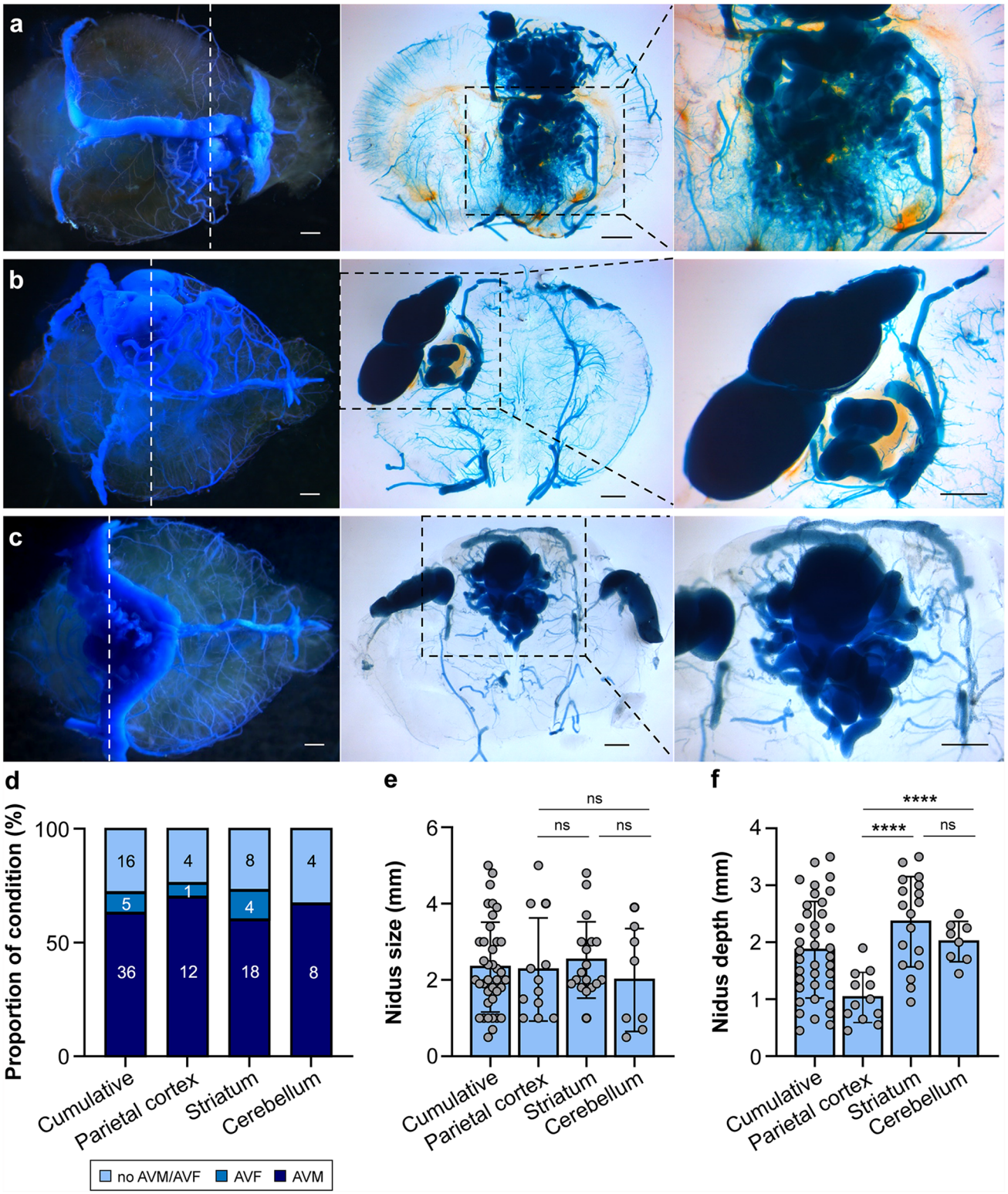

Fig. 1 Localized induction of brain AVMs in a mouse model of HHT. Representative microscopy imaging showing latex dye-perfused brains with brain AVMs in the right-side striatum (*white dashed lines* show slice location) (**a**), left-side parietal cortex (**b**), and midline cerebellum (**c**). Whole brain (*left*) and low-magnification (*center*; *black dashed lines* indicate areas of magnification) and high-magnification (*right*) coronal section images. Bar, 1 mm. **d** Bar graph representing frequencies of brain AVM development after stereotaxic intracerebral injection of 4-OHT into the striatum, parietal cortex, and cerebellum. Mean (SD). Bar graphs representing the nidus size (**e**) and lesion depth (**f**) after stereotaxic intracerebral injection of 4-OHT into the striatum, parietal cortex, and cerebellum. Mean (SD), ANOVA. ****$p < 0.001$; *ns* not significant

mm, $p < 0.001$) (Fig. 1f). Brain AVMs formed in the target injection region with 98% (40/41) accuracy; thus, all brain AVMs developed at or near the injection site and in the intended hemisphere (parietal cortex, left hemisphere; striatum, right hemisphere) or along the midline (cerebellum). One mouse was injected into the midline cerebellum but was identified as having formed a brain AVM in the right anterior hemisphere in subcortical structures.

Most brain AVMs were associated with various degrees of intracranial microhemorrhage. Five mice presented with hydrocephalus clinically evident as reduced mobility, apathy, and increased head circumference. The presence of hydrocephalus was confirmed in all 5 after perfusion with latex dye (Supplemental Fig. 2a). One mouse in the longitudinal analysis gradually developed radiographic signs of hydrocephalus starting at 5 months of age without clinical evidence of increased intracranial pressure (Supplemental Fig. 2b).

Validation of injection site-specific genetic recombination

Using our stereotaxic injection protocol in $R26^{CreER/mTmG}$;$Alk1^{2f/2f}$ reporter mice, we sought to visualize the extent of genetic recombination induced in the mouse brain by the technique. In mT/mG reporter mice, mT labeling (TdTomato) is constitutively expressed and replaced with mG labeling (GFP fluorescence) upon activation of Cre. Among 6 mutant $R26^{CreER/mTmG}$;$Alk1^{2f/2f}$ mice that received a single dose of 4-OHT into the left parietal cortex, 4 developed brain AVMs, and all had Cre-mediated mG labeling adjacent to the lesion margin in the brain cortex (Supplemental Fig. 3). GFP fluorescence was not detectable in 2 mutants that had not formed brain AVMs, suggesting that no genetic recombination occurred in mice that did not form brain AVMs.

Timing of brain AVM development

Although several mouse models simulate adult-onset brain AVM formation [14, 15], modeling brain AVMs in the postnatal period is less established. We sought to investigate the timing of brain AVM development in this model. Brain AVMs started forming as early as 1 week postinjection of 4-OHT and displayed a premature phenotype with tortuous vessel formation while remaining small (Fig. 2a). In contrast, brain AVMs analyzed 2 and 3 weeks postinjection gradually increased in size and displayed a mature and complex nidal phenotype (Fig. 2b and c).

Intracerebral versus systemic conditional gene deletion

The systemic activation of Cre in conditional knockout mice results in micro- and macrohemorrhaging from AVMs in internal organs [12, 17]. To showcase the effect differences of intracerebral versus systemic Cre activation, we treated neonatal *Alk1*-iKO mice (P1) with tamoxifen by intragastric injection (50 mg/kg body weight). The intragastric application of tamoxifen in neonatal *Alk1*-iKO mice was associated with an immediate 100% mortality rate within the first week of life in all mice ($n = 5$), exemplifying the potency of ubiquitous *Alk1* deletion through systemic Cre activation. Therefore, we adapted our experimental design to administer tamoxifen to 4-week-old *Alk1*-iKO mice by intraperitoneal injection (200 mg/kg body weight). 1 week posttreatment, the hemoglobin levels of systemically tamoxifen-treated *Alk1*-iKO mice were analyzed and compared to stereotactically 4-OHT-injected *Alk1*-iKO mice. Systemically treated *Alk1*-iKO mutants had significantly decreased hemoglobin levels compared to control mice (15.98 g/dL vs. 5.67 g/dL, $p < 0.001$) and compared to stereotactically treated *Alk1*-iKO mutants (13.31 g/dL vs. 5.67 g/dL, $p < 0.001$) (Supplemental Fig. 4a). Mean (SD) hemoglobin levels were not statistically different between stereotactically injected *Alk1*-iKO mutant and control mice (13.31 g/dL vs. 13.97 g/dL, $p = 2.0$). Based on the hemoglobin analysis, stereotaxic injection of 4-OHT was restricted to producing AVMs in the brain, whereas the systemic injection of tamoxifen was associated with the development of AVMs in the ears, cecum, and stomach (Supplemental Fig. 4b).

Longitudinal HHT mouse model of brain AVMs

After stereotaxic injection of 4-OHT into the left parietal cortex, 7 *Alk1*-iKO mice were identified as having developed vascular lesions on 1-month magnetic resonance angiography (MRA) imaging and were included for longitudinal analysis (Table 1). Control mice displayed normal cerebrovasculature (Fig. 3a). All brain AVMs developed in the left parietal cortex. Four mice formed large nidal AVMs, 1 formed a small nidal AVM, 1 an AVF, and 1 an extracranial–intracranial AVM. One mouse with a large nidal AVM died at 2 months of age, likely due to spontaneous AVM rupture; 1 mouse developed aggressive behavior warranting early termination; and a 9-month-old mouse with a large nidal AVM developed progressive face swelling, likely due to venous congestion. Four of 7 mice were alive at the end of the mean (SD; range) study period of 7.2 (3; 2.3–9.5) months. However, after accounting for the event of necessary

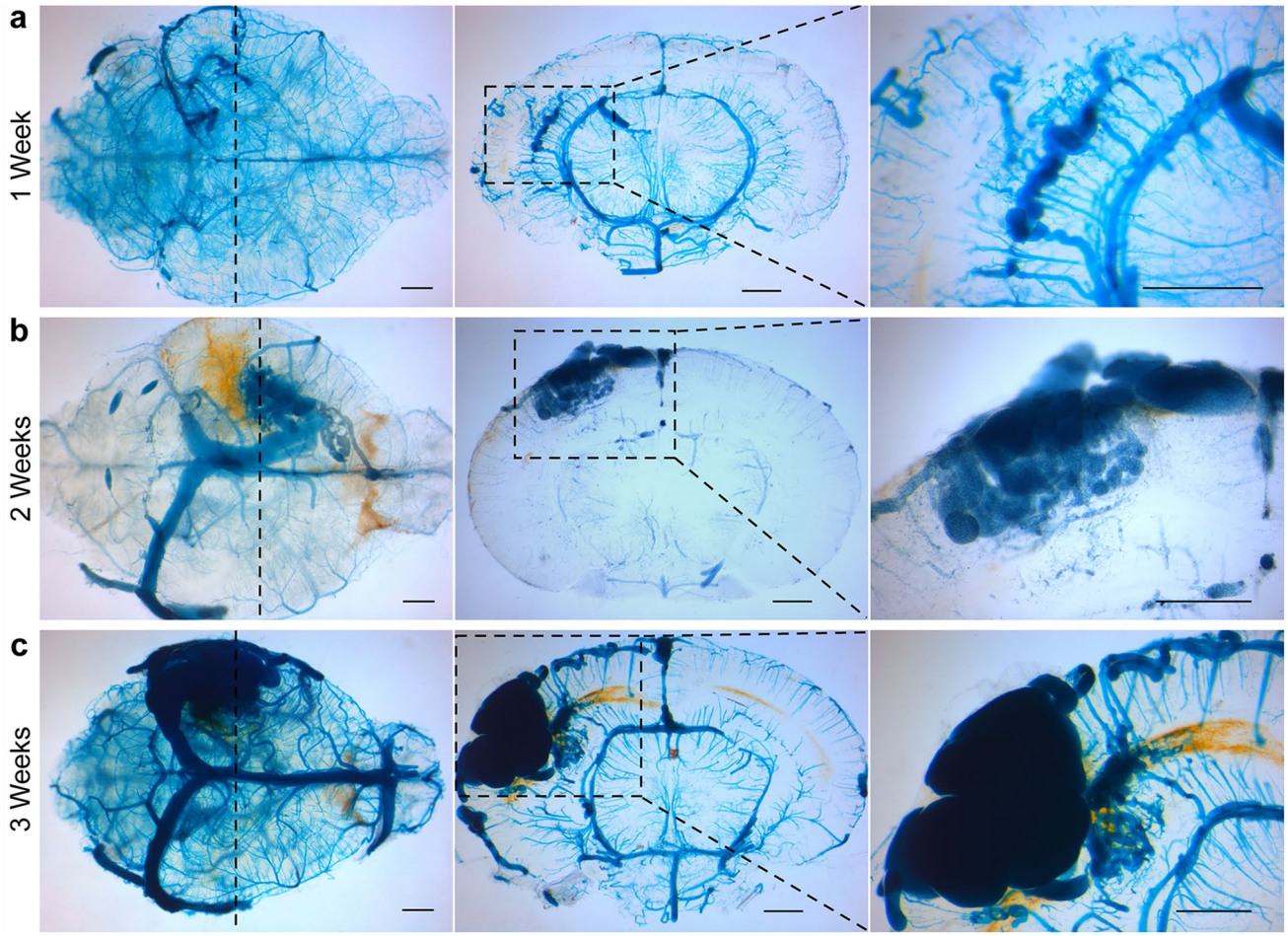

Fig. 2 Timing of brain AVM development after stereotaxic intracerebral injection of 4-OHT in *Alk1*-inducible knockout mice. **a** Microscopy images of latex dye-perfused brains showing a brain AVM in the parietal cortex 7 days postinjection ($n=3$). **b** Microscopy images showing a brain AVM in the parietal cortex 14 days postinjection ($n=2$). **c** Microscopy images showing a brain AVM in the parietal cortex 21 days postinjection ($n=5$). Whole brain (*left; dashed line* shows location) and low-magnification (*center*; *black outlines* indicate area of magnification) and high-magnification (*right*) coronal section images. Bar, 1 mm

Table 1 Analysis of 3D MR gradient echo flow compensation angiograms

Mouse no.	Vascular lesion	Age (months)	Sex	Target location	Nidus size (mm)	Compactness
1	AVM	9.4	M	L parietal cortex	4.54	Compact
2	AVM	5.1	M	L parietal cortex	4.80	Compact
3	AVM	9.2	F	L parietal cortex	5.21	Compact
4	AVM	9.4	M	L parietal cortex	2.56	Compact
5	AVM	2.3	F	L parietal cortex	4.47	Diffuse
6	AVM	5.1	M	L parietal cortex	3.90	Diffuse
7	AVF	9.4	M	L parietal cortex	N/A	N/A

early termination, the long-term survival rate of this model was 75% (4/5) at 9 months. Brain AVM nidi were grossly stable on serial 3D time-of-flight MRA, with radiographic evidence of remodeling between 1 and 3 months after the onset of brain AVM development (Fig. 3b).

Histological characterization of brain AVMs

The morphological hallmarks of human brain AVMs include the complexity of nidus formation, recurrent microhemorrhages, and invasion of immune cells leading to focal inflammation [18]. To confirm the presence of these hallmarks

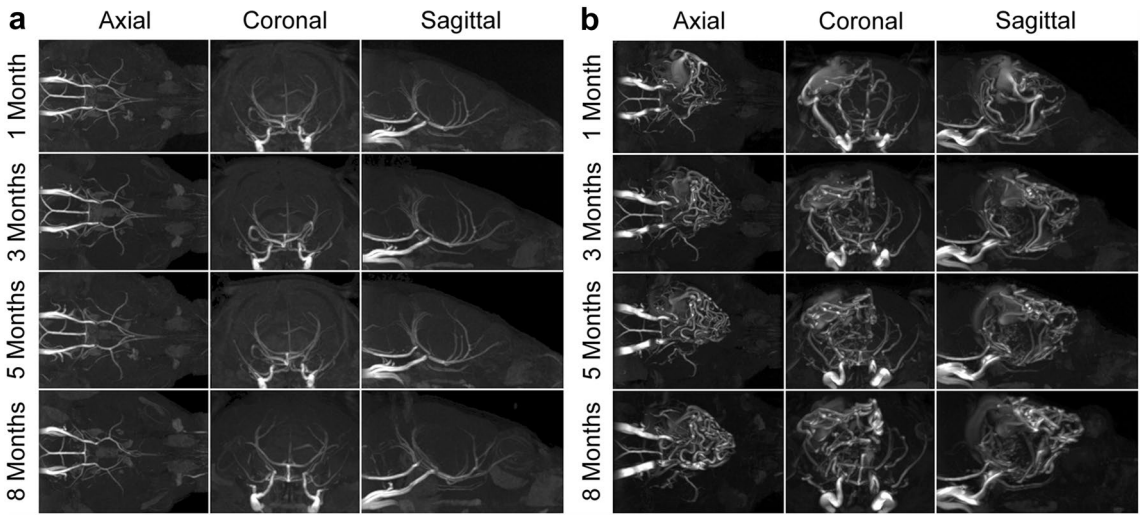

Fig. 3 Longitudinal MRA of a brain AVM in an HHT mouse model. **a** MRA imaging showing axial (*left*), coronal (*center*), and sagittal (*right*) views of a control mouse brain with normal angioarchitecture at 1, 3, 5, and 8 months. **b** MRA imaging showing axial (*left*), coronal (*center*), and sagittal (*right*) views of a large nidal brain AVM in the left-side parietal cortex at 1, 3, 5, and 8 months

in our mouse model, we performed immunohistochemical staining on a 3-month-old mouse brain with an AVM confirmed with 3D time-of-flight MRA (Fig. 4a) and 2D MRA imaging (Fig. 4b). Prussian blue staining showed microhemorrhages centered in the brain AVM nidus and surrounding this vasculature (Fig. 4c). Microhemorrhages correlated with a diffuse pattern of CD68-positive cells surrounding the nidal vessels, which were not detected in control brains (Fig. 4d). Multifluorescent immunostaining for endothelial cells (CD31) and smooth muscle cells (SMA) showed complex nidal vasculatures in coronal brain tissue sections, which were absent in controls (Fig. 4e).

Discussion

Brain AVMs are an important cause of hemorrhagic stroke, with limited availability of safe and effective, noninvasive treatment options to prevent them from bleeding [19, 20]. Our understanding of the detailed mechanisms underlying disease progression remains enigmatic. There is a lack of high-fidelity mouse models that (1) produce brain AVMs with high efficiency and without lethal off-target effects, (2) produce brain AVMs with a high degree of similarity with the human disease pathology, and (3) permit longitudinal disease modeling. We present the first HHT mouse model that allows for targeted induction of brain AVMs in transgenic mice using stereotaxic intracerebral injection of 4-OHT. The results demonstrate a robust longitudinal mouse model that closely mimics the pathobiological hallmarks of human brain AVMs, including microhemorrhage, immune cell invasion, nidus formation, and spontaneous rupture.

Mouse model of familial brain AVMs in context

Our group previously developed a longitudinal HHT mouse model using *Tagln*-Cre;*Alk1*$^{2f/2f}$ transgenic mice and characterized the vascular lesions histologically and radiographically [12]. This model is based on the conditional genetic deletion of *Alk1* during embryogenesis, which led to the development of nidal brain AVMs in 40% of mice, AVFs in 18%, and no vascular lesions in 42%. On high-resolution digital subtraction angiography, the model recapitulated the radiographic key features of human disease, including early arteriovenous shunting, complex nidus angioarchitecture, microhemorrhages, and nidal stability for a mean duration of 9.5 months (range, 3–17 months). However, we noted a 4-week mortality of 20% and an additional 35% mortality by the age of 6 months, likely related to hemorrhages in the gastrointestinal tract, lungs, and brain. One of the key advantages of our mouse model is the reduction of mortality rates compared to traditional models. This reduction was achieved by avoiding side effects related to the systemic administration of tamoxifen, such as anemia and multisite hemorrhages due to ubiquitous Cre activation, producing improved long-term survival.

Walker et al. developed a mouse model that employed stereotaxic intracranial delivery of adenoviral vector—expressing Cre recombinase combined with an adeno-associated viral vector expressing vascular endothelial growth factor (VEGF) to generate brain AVMs in adult *Alk1*$^{2f/2f}$ mice [14]. Unlike our model, which primarily produced a

complex vascular nidus, the Walker et al. model is characterized by increased vessel density and vascular dysplasia as the primary pathological features. The phenotypical hallmark of complex nidus formation is disease-specific and essential for deciphering the cellular and molecular changes underlying altered hemodynamics in brain AVMs. These features provide accurate and reliable representations of the pathology seen in humans. Zhu et al. used CRISPR/Cas9 technology to locally introduce somatic endothelial cell-specific *Alk1* gene mutations in brains of adult wild-type mice [21]. An adeno-associated viral vector expressing VEGF was coadministered for angiogenesis in these mouse brains. The model produced arteriovenous shunts with an increased vessel dysplasia index but without a true vascular nidus.

Another approach to creating a mouse model of brain AVMs is to induce somatic activating *KRAS* mutations, which have been implicated in the pathogenesis of human sporadic brain AVMs [22–25]. The viral-mediated endothelial cell-specific overexpression of mutant $KRAS^{G12V}$ protein generated multiple small nidi in the mouse brain [25]. These nidi were accompanied by additional characteristics, including upregulation of endogenous VEGF signaling, spontaneous multifocal intracerebral hemorrhages, neuroinflammation, and sensory, cognitive, and motor behavior dysfunction [25]. Although this approach provides valuable insights into the underlying mechanisms of sporadic brain AVMs, it might not be applicable to study the genetic interactions that occur in familial brain AVMs.

Our mouse model provides a short latency and AVM production without angiogenic stimulation or highly complex genetic engineering techniques. The vascular lesions are detectable 1 week postprocedure, with progressive maturation into complex nidal brain AVMs by 3 to 4 weeks of age, and are associated with markedly elevated neuroinflammation. These features distinguish our mouse model from others [14, 15, 21, 25–27], requiring costly genetic engineering techniques, long latency times, and additional angiogenic stimulation to induce brain AVMs.

Technical aspects

Intracranial stereotaxic injection is a technique used to deliver substances to specific brain regions with high spatial precision. The technique has been employed in many experimental settings, including glioblastoma [28], posttraumatic epilepsy [29], multiple sclerosis [30], Alzheimer's disease [31], and intracranial aneurysm formation and rupture [32]. The advantages of disease induction by stereotaxic injection are high precision, easy applicability, and versatility. Varying degrees of interperformer or intersubject variability may be observed [33]. The technique is relatively noninvasive, which minimizes stress on the animal and reduces the risk of periprocedural complications. The procedure was associated with a low rate of adverse outcomes, most commonly intracerebral hemorrhage due to injury of the dural venous sinus.

Brain AVM characteristics

The model's validity has been established through histological and radiographic characterizations, showing that the mouse brain AVMs closely mimic the characteristics and pathology of human brain AVMs. Pathological hallmarks include the formation of a vascular nidus with complex angioarchitecture and arteriovenous shunting with vessel enlargement and tortuosity, microhemorrhages with associated neuroinflammation, and longitudinal nidal stability, with features of radiographically evident remodeling during the early stages of AVM maturation [18, 34–36].

The occurrence of hydrocephalus in mice with large, hemorrhagic brain AVMs is notable. The association between hydrocephalus and brain AVMs is well established and is a common presenting symptom of human pediatric brain AVMs [37]. However, it is seen in less than 1% of adults with AVMs [38, 39]. Hydrocephalus is most often caused by intraventricular hemorrhage, which results in malabsorption-type hydrocephalus [40]. In unruptured brain AVMs, the most common pathogenic mechanisms of hydrocephalus involve mechanical obstruction by the draining vein or AVM nidus or venous congestion [37]. Because all hydrocephalic mice in this study had large nidal brain AVMs with microhemorrhages, malabsorption caused by blockage of the arachnoid granulations could be implicated in the pathogenesis of hydrocephalus, along with mechanical venous or ventricular obstruction.

Limitations

The model's limitations relate to technical and precision challenges. Although we demonstrated spatial lesion variability in various brain areas, we could not induce uniformly sized lesions in all brain regions. This phenomenon was likely due to the limited solubility of 4-OHT in water, making it difficult to achieve consistent and uniform dosing across all animals. Furthermore, the long-term survival might not accurately reflect the true survival rate of the model due to the small sample size and possible early terminations. Despite these limitations, the minimal rates of early lethality associated with localized Cre induction portend excellent long-term survival rates compared to other mouse models.

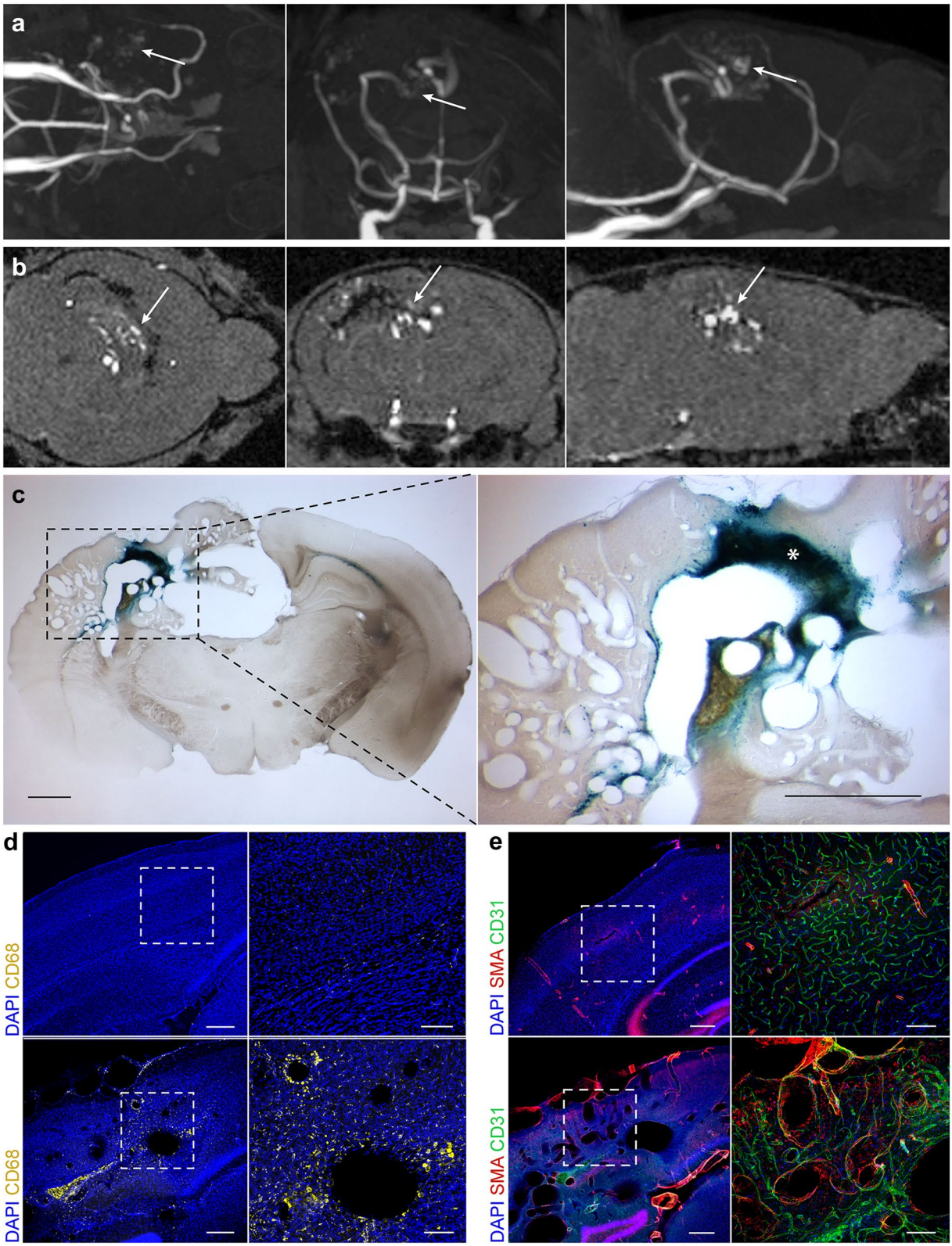
a
b
c
*
d
DAPI CD68
DAPI CD68
e
DAPI SMA CD31
DAPI SMA CD31

◂**Fig. 4** Histological analysis of brain AVMs in *Alk1*-inducible knockout mice induced by stereotaxic intracerebral injection of 4-OHT. **a** 3-Dimensional and 2-dimensional **b** time-of-flight MRA imaging showing axial (*left*), coronal (*center*), and sagittal (*right*) views of a brain AVM at 3 months of age. *White arrows* indicate location of the brain AVM. **c** Microscopy images of coronal mouse brain tissue section after Prussian blue staining showing microhemorrhages surrounding the nidal vasculature. *Area of ferric iron deposition. Low-magnification (*left*; *dashed black outlines* indicate area of magnification; bar 1 mm) and high-magnification (*right*, bar 1 mm) coronal section images. **d** Coronal mouse brain tissue section of control (*top* panels) and *Alk1*-inducible knockout (*bottom* panels) mouse after immunostaining for monocytes/macrophages (CD68). Low-magnification (*left*; *white outlines* indicate area of magnification, bar 250 µm) and high-magnification (*right*, bar 100 µm) coronal section images. **e** Coronal mouse brain tissue section of control (*top* panels) and *Alk1*-inducible knockout (*bottom* panels) mouse after immunostaining for endothelial cells (CD31) and alpha-SMA. Low-magnification (*left*; *white outlines* indicate area of magnification, bar 250 µm) and high-magnification (*right*, bar 100 µm) coronal section images

Conclusion

We present the first mouse model of HHT with localized induction of brain AVMs through stereotaxic CreER-mediated genetic recombination. The model efficiently produces brain AVMs while bypassing drivers of early morbidity and mortality. The lesions closely resemble human disease pathology, including complex nidus formation with arteriovenous shunts, microhemorrhages, immune cell infiltration, and nidal stability. Notable technical advantages of this model include its easy applicability, versatility, and no need for angiogenic stimulation. The model's capacity to reliably reproduce brain AVM in various brain regions and its robustness in recapitulating disease progression over time make it a valuable tool to reveal the pathological mechanisms underlying brain AVM formation and develop novel therapeutic strategies with accelerated translation.

Supplementary information The online version contains supplementary material available at https://doi.org/10.1007/s10456-023-09881-w.

Acknowledgements We thank Alberto E. Fuentes and Gregory H. Turner for technical assistance with magnetic resonance imaging. We also thank Dakota T. Graham for providing the 3D-printed mouse neonatal stereotaxic adapter from the Barrow Innovation Center at Barrow Neurological Institute. We thank the staff of Neuroscience Publications at Barrow Neurological Institute for assistance with manuscript preparation.

Author contributions LS performed experiments, analyzed the data and wrote the first draft; CH, YHK and TDS performed experiments; EAW and JSC assisted with data analysis; PV edited the manuscript; MTL and SPO designed and supervised the entire project.

Funding This work was supported by the Barrow Neurological Foundation, Leducq Foundation (ATTRACT), and the Department of Defense (PR161205).

Declarations

Competing interests The authors have no personal, financial, or institutional interest in any of the drugs, materials, or devices described in this manuscript.

References

1. Stapf C, Labovitz DL, Sciacca RR, Mast H, Mohr JP, Sacco RL (2002) Incidence of adult brain arteriovenous malformation hemorrhage in a prospective population-based stroke survey. Cerebrovasc Dis 13:43–46
2. van Beijnum J, Lovelock CE, Cordonnier C, Rothwell PM, Klijn CJ, Al-Shahi Salman R et al (2009) Outcome after spontaneous and arteriovenous malformation-related intracerebral haemorrhage: population-based studies. Brain 132:537–543
3. Shaligram SS, Winkler E, Cooke D, Su H (2019) Risk factors for hemorrhage of brain arteriovenous malformation. CNS Neurosci Ther 25:1085–1095
4. Lawton MT, Rutledge WC, Kim H, Stapf C, Whitehead KJ, Li DY et al (2015) Brain arteriovenous malformations. Nat Rev Dis Primers 1:15008
5. Roman BL, Hinck AP (2017) Alk1 signaling in development and disease: new paradigms. Cell Mol Life Sci 74:4539–4560
6. Brinjikji W, Iyer VN, Sorenson T, Lanzino G (2015) Cerebrovascular manifestations of hereditary hemorrhagic telangiectasia. Stroke 46:3329–3337
7. Brinjikji W, Iyer VN, Wood CP, Lanzino G (2017) Prevalence and characteristics of brain arteriovenous malformations in hereditary hemorrhagic telangiectasia: a systematic review and meta-analysis. J Neurosurg 127:302–310
8. Tual-Chalot S, Oh SP, Arthur HM (2015) Mouse models of hereditary hemorrhagic telangiectasia: recent advances and future challenges. Front Genet 6:25
9. Urness LD, Sorensen LK, Li DY (2000) Arteriovenous malformations in mice lacking activin receptor-like kinase-1. Nat Genet 26:328–331
10. Li DY, Sorensen LK, Brooke BS, Urness LD, Davis EC, Taylor DG et al (1999) Defective angiogenesis in mice lacking endoglin. Science 284:1534–1537
11. Ola R, Dubrac A, Han J, Zhang F, Fang JS, Larrivee B et al (2016) Pi3 kinase inhibition improves vascular malformations in mouse models of hereditary haemorrhagic telangiectasia. Nat Commun 7:13650
12. Han C, Lang MJ, Nguyen CL, Luna Melendez E, Mehta S (2021) Turner GH et al Novel experimental model of brain arteriovenous malformations using conditional alk1 gene deletion in transgenic mice. J Neurosurg. https://doi.org/10.3171/2021.6.JNS21717

13. Ola R, Kunzel SH, Zhang F, Genet G, Chakraborty R, Pibouin-Fragner L et al (2018) Smad4 prevents flow induced arteriovenous malformations by inhibiting casein kinase 2. Circulation 138:2379–2394
14. Walker EJ, Su H, Shen F, Degos V, Amend G, Jun K et al (2012) Bevacizumab attenuates vegf-induced angiogenesis and vascular malformations in the adult mouse brain. Stroke 43:1925–1930
15. Choi EJ, Chen W, Jun K, Arthur HM, Young WL, Su H (2014) Novel brain arteriovenous malformation mouse models for type 1 hereditary hemorrhagic telangiectasia. PLoS ONE 9:e88511
16. Chen W, Young WL, Su H (2014) Induction of brain arteriovenous malformation in the adult mouse. Methods Mol Biol 1135:309–316
17. Park SO, Wankhede M, Lee YJ, Choi EJ, Fliess N, Choe SW et al (2009) Real-time imaging of de novo arteriovenous malformation in a mouse model of hereditary hemorrhagic telangiectasia. J Clin Investig 119:3487–3496
18. Winkler EA, Kim CN, Ross JM, Garcia JH, Gil E, Oh I et al (2022) A single-cell atlas of the normal and malformed human brain vasculature. Science 375:eabi7377
19. Winkler EA, Lu AY, Raygor KP, Linzey JR, Jonzzon S, Lien BV et al (2019) Defective vascular signaling & prospective therapeutic targets in brain arteriovenous malformations. Neurochem Int 126:126–138
20. Robert F, Desroches-Castan A, Bailly S, Dupuis-Girod S, Feige JJ (2020) Future treatments for hereditary hemorrhagic telangiectasia. Orphanet J Rare Dis 15:4
21. Zhu W, Saw D, Weiss M, Sun Z, Wei M, Shaligram S et al (2019) Induction of brain arteriovenous malformation through crispr/cas9-mediated somatic alk1 gene mutations in adult mice. Transl Stroke Res 10:557–565
22. Nikolaev SI, Vetiska S, Bonilla X, Boudreau E, Jauhiainen S, Rezai Jahromi B et al (2018) Somatic activating kras mutations in arteriovenous malformations of the brain. N Engl J Med 378:250–261
23. Fish JE, Flores Suarez CP, Boudreau E, Herman AM, Gutierrez MC, Gustafson D et al (2020) Somatic gain of kras function in the endothelium is sufficient to cause vascular malformations that require mek but not pi3k signaling. Circ Res 127:727–743
24. Hong T, Yan Y, Li J, Radovanovic I, Ma X, Shao YW et al (2019) High prevalence of kras/braf somatic mutations in brain and spinal cord arteriovenous malformations. Brain 142:23–34
25. Park ES, Kim S, Huang S, Yoo JY, Körbelin J, Lee TJ et al (2021) Selective endothelial hyperactivation of oncogenic kras induces brain arteriovenous malformations in mice. Ann Neurol 89:926–941
26. Chen W, Sun Z, Han Z, Jun K, Camus M, Wankhede M et al (2014) De novo cerebrovascular malformation in the adult mouse after endothelial alk1 deletion and angiogenic stimulation. Stroke 45:900–902
27. Choi E-J, Walker EJ, Shen F, Oh SP, Arthur HM, Young WL et al (2012) Minimal homozygous endothelial deletion of eng with vegf stimulation is sufficient to cause cerebrovascular dysplasia in the adult mouse. Cerebrovasc Dis 33:540–547
28. Jun HJ, Appleman VA, Wu HJ, Rose CM, Pineda JJ, Yeo AT et al (2018) A pdgfralpha-driven mouse model of glioblastoma reveals a stathmin1-mediated mechanism of sensitivity to vinblastine. Nat Commun 9:3116
29. Das J, Singh R, Sharma DJNN (2017) Antiepileptic effect of fisetin in iron-induced experimental model of traumatic epilepsy in rats in the light of electrophysiological, biochemical, and behavioral observations. Nutr Neurosci 20:255–264
30. Merkler D, Ernsting T, Kerschensteiner M, Brück W, Stadelmann CJB (2006) A new focal eae model of cortical demyelination: multiple sclerosis-like lesions with rapid resolution of inflammation and extensive remyelination. Brain 129:1972–1983
31. Jean YY, Baleriola J, Fà M, Hengst U, Troy CM (2015) Stereotaxic infusion of oligomeric amyloid-beta into the mouse hippocampus. J Vis Exp: JoVE. https://doi.org/10.3791/52805
32. Tada Y, Kanematsu Y, Kanematsu M, Nuki Y, Liang EI, Wada K et al (2011) A mouse model of intracranial aneurysm: technical considerations. Acta Neurochir Suppl 111:31–35
33. Narayanan DP, Tsukano H, Kline AM, Onodera K, Kato HK (2022) Biological constraints on stereotaxic targeting of functionally-defined cortical areas. Cereb Cortex. https://doi.org/10.1093/cercor/bhac275
34. Chen Y, Zhu W, Bollen AW, Lawton MT, Barbaro NM, Dowd CF et al (2008) Evidence of inflammatory cell involvement in brain arteriovenous malformations. Neurosurgery 62:1340–1350
35. Geibprasert S, Pongpech S, Jiarakongmun P, Shroff MM, Armstrong DC, Krings T (2010) Radiologic assessment of brain arteriovenous malformations: what clinicians need to know. Radiographics 30:483–501
36. Wright R, Jarvelin P, Pekonen H, Keranen S, Rauramaa T, Frosen J (2020) Histopathology of brain avms part ii: inflammation in arteriovenous malformation of the brain. Acta Neurochir (Wien) 162:1741–1747
37. Geibprasert S, Pereira V, Krings T, Jiarakongmun P, Lasjaunias P, Pongpech S (2009) Hydrocephalus in unruptured brain arteriovenous malformations: pathomechanical considerations, therapeutic implications, and clinical course. J Neurosurg 110:500–507
38. Pribil S, Boone S, Waley R (1983) Obstructive hydrocephalus at the anterior third ventricle caused by dilated veins from an arteriovenous malformation. Surg Neurol 20:487–492
39. Mindea S, Yang B, Batjer H (2007) Unruptured arteriovenous malformation in a patient presenting with obstructive hydrocephalus. Case Rep Rev Lit 22:E11
40. Choi JH, Mohr JPJTLN (2005) Brain arteriovenous malformations in adults. Lancet Neurol 4:299–308

Authors and Affiliations

Lea Scherschinski[1,2,3] · Chul Han[1] · Yong Hwan Kim[1] · Ethan A. Winkler[1,2] · Joshua S. Catapano[2] · Tyler D. Schriber[1] · Peter Vajkoczy[3] · Michael T. Lawton[1,2] · S. Paul Oh[1]

✉ S. Paul Oh
ohp@barrowneuro.org

[1] Department of Translational Neuroscience, Barrow Aneurysm and AVM Research Center, St. Joseph's Hospital and Medical Center, Barrow Neurological Institute, 350 W. Thomas Rd., Phoenix, AZ 85013, USA

[2] Department of Neurosurgery, St. Joseph's Hospital and Medical Center, Barrow Neurological Institute, Phoenix, AZ, USA

[3] Department of Neurosurgery, Charité – Universitätsmedizin Berlin corporate member of Freie Universität Berlin, Humboldt-Universität zu Berlin, Berlin Institute of Health, Berlin, Germany